9th International Conference on HYDROELASTICITY IN MARINE TECHNOLOGY
Rome, Italy, July 10th-13th, 2022

A FLOATING MEMBRANE SOLAR ISLAND STUDY

Kristiansen, T.[1*], Grøn, P.[1,3] and Faltinsen, O. M.[2]

[1] Dept. of Marine Technology, Norwegian University of Science and Technology (NTNU), Trondheim, Norway (trygve.kristiansen@ntnu.no)
[2] Centre for Autonomous Marine Operations and Systems (NTNU AMOS), Trondheim, Norway
[3] OceanSun, Oslo, Norway

Abstract. We present work towards a rational model of a floating membrane solar island: a floating circular membrane is attached to an elastic torus. Dedicated experiments are performed in a wave flume. Numerical work is carried out within the framework of linearized potential flow theory. The island is modelled as two connected bodies, using generalized modes in the panel code WAMIT. The membrane is assumed to obey the linear membrane equation with pre-tension. The elastic torus obeys a curved Euler-Bernoulli beam equation. Compatibility along the membrane rim is modelled with a Lagrange multiplier method. Response Amplitude Operators (RAOs) are presented for several vertical modes and points on the membrane. Several of the lowest mode RAOs compare very well, but there are clear discrepancies in higher modes and at points near the membrane rim for waves that are shorter than the membrane diameter. The reason is believed to be an unsatisfactory modelling of the membrane connection to the floater. The hydrostatic term is important, but membrane pre-tension matters. Tank wall reflections in the experiments matter. The island follows the waves to a great extent, but nonlinear effects are relevant with respect to over-topping.

Key words: Floating membrane; Elastic torus; Hydroelasticity; Floating solar island

1. Introduction

Floating solar has the potential to contribute significantly to the future, renewable energy mix. Solar islands may be installed on inland reservoirs, hydropower dams, near-shore locations at sea and more exposed locations. The different levels of wave and wind exposure calls for a variety of solar island concepts. Common to all is that they must be highly cost-efficient, while at the same time be able to endure the environmental loads. The structure must be able to follow the waves in relevant sea states to minimize green water and bottom impact. A consequence is that hydroelastic structures have been studied. Different proposed and available types include multi-modular type [1], multi-torus type [2] and membrane-based islands [3]. In the present work we consider a circular, floating membrane supported by an elastic floater, inspired by [3]. Our work represents a step towards a rational model with the purpose of predicting different important responses such as mooring loads, vertical and horizontal membrane motions, possible slack with resulting snap loads, and over-topping of waves. For some of these responses nonlinear effects matter, and the model should be further developed in future work. Dedicated model tests were carried out and these are presented first. Next, a numerical model based on linear membrane and torus equations and linear potential flow theory is presented. We solve the hydrodynamic problem numerically using generalized modes in WAMIT. An alternative could be to attempt a semi-analytic solution, such as for instance [4], but hydrodynamic interaction between the floater and the membrane would need to be accounted for. Results are compared and discussed with focus on apparent discrepancies and needs for more complete and detailed modelling.

* Correspondence to: trygve.kristiansen@ntnu.no

1. Model tests

Our model tests were carried out in the Small Towing Tank at NTNU during 2021. The tank is 26 m long and 2.5 m wide. The water depth was 0.7 m. The model was moored with four near horizontal mooring lines, angled 45° to the incident waves, with a pulley and vertical spring attached to the tank walls. The set-up is show schematically in Figure 1. Two snapshots of the model in an irregular sea state are provided in Figure 2.

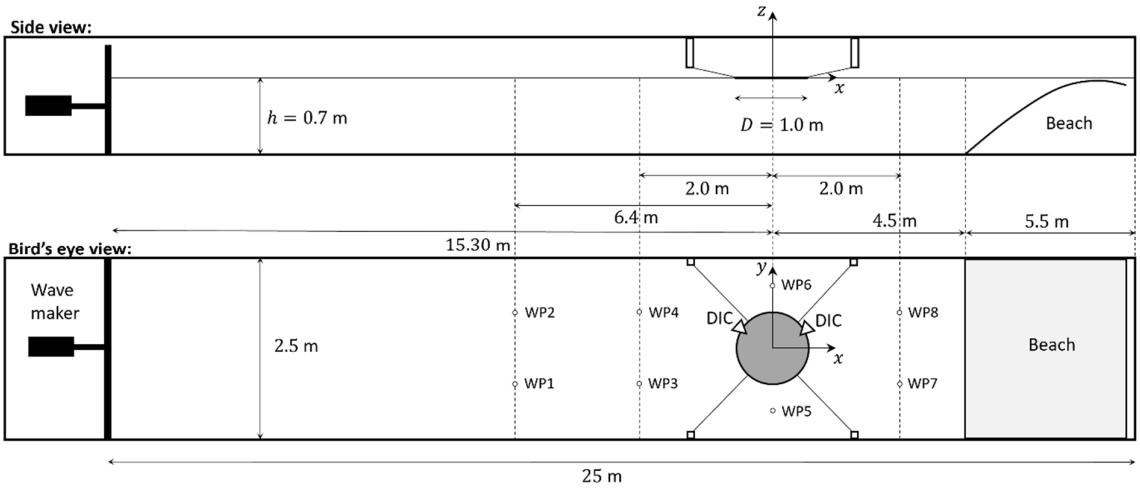

Figure 1. Experimental set-up of a floating membrane solar island model in the Small Towing Tank at NTNU in Trondheim.

The total model diameter was $D = 2R = 1.0$ m (center-axis of the floater) and was made of a thin rubber membrane and elastic pipe that were connected by an arrangement of 32 equidistant steel clips and rubber bands. See Figure 3. The membrane was wrapped vertically at its rim to avoid flooding of water, and the diameter of the flat part of the membrane in contact with water was approximately 0.96 m. A ribbon was glued on the outside of the membrane to facilitate pre-tensioning. The band was relatively stiff. Measurement of the bending stiffness EI_m was attempted, with values provided in Table 1 along with other main model parameters. This includes the effect of membrane wrap and the steel handrail in addition to the ribbon.

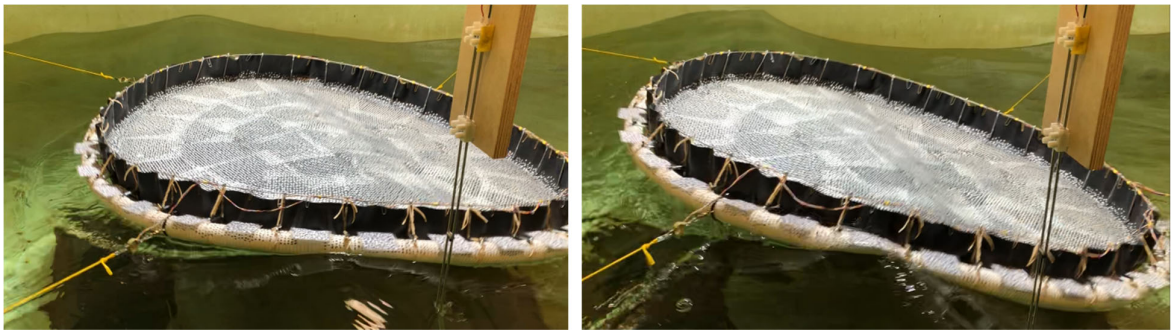

Figure 2. Two snapshots of the model subjected to irregular waves (from left). The sea state corresponds to $H_s = 4.5$ m, $T_p = 9$ s, considering a model scale of 1:50 and Froude scaling. In this sea-state, the floater goes out of water in the front part. In our regular wave tests, this, or water-on-deck was not observed.

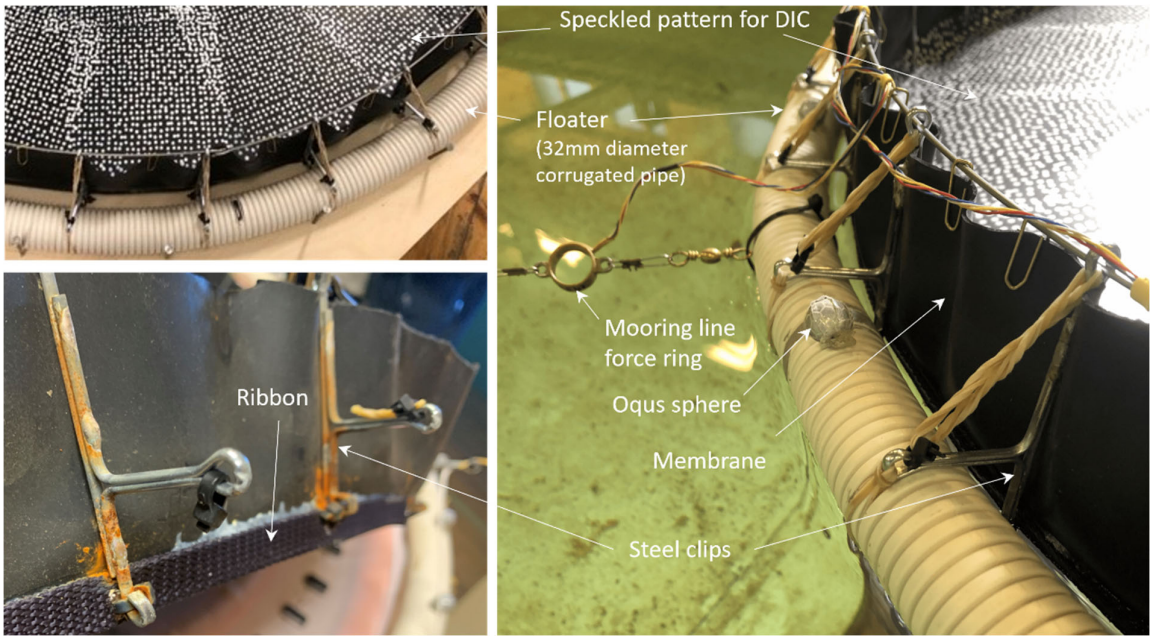

Figure 3. Three close-up photos of the model consisting of a rubber-material membrane connected to an elastic floater by steel clips and rubber bands. The membrane rim was wrapped vertically to avoid flooding by waves. The speckle pattern was used for the Digital Image Correlation (DIC) system which non-intrusively measures both out-of-the plane (near vertical) motions as well as in-plane strain.

The horizontal and vertical (flexible) motions of the island model were measured by two motion capturing systems: Qualisys Oqus motion capture and a Digital Image Capturing (DIC) system by Correlated Solutions. The Oqus system was used to measure the motion of selected points along the elastic floater motions as well as one point near the center of the membrane, by means of reflective spheres. One such reflective sphere is shown in Figure 3. The DIC system was used to measure the membrane motions. The position of the two DIC cameras are indicated in Figure 1. The membrane was speckled for pattern recognition as shown in Figure 3. For practical reasons due to shadowing and light reflections, successful DIC data were acquired for one half only, and not all the way to the rim; $y \geq 0$, $r \leq 0.4$ m. Here, r is the radial distance from the model center, as shown in Figure 4. Force rings were attached to all four mooring lines.

Table 1. Main parameters of the model set-up in the present experiments at NTNU.

Model diameter (center axis of the floater)	$D = 2R$	1.00 [m]
Floater cross-sectional diameter (largest/outer diameter of the corrugated pipe)	$2a$	0.032 [m]
Membrane thickness	t	0.0011 [m]
Mooring stiffness of each spring	k_s	28 [N/m]
Membrane mass	M_m	1.30 [kg]
Total island mass	M_t	2.18 [kg]
Floater bending stiffness	EI_f	0.11 [N/m^2]
Vertical bending stiffness membrane rim seem	EI_m	$0.22 - 0.30$ [N/m^2]

The model was subjected to both regular and irregular waves, but no current. The regular wave tests included four different wave steepnesses, H/λ, out of which DIC was applied only to the highest and lowest steepness, and a large range of wavelength- to model-diameter ratios. Here, H refer to (linear) wave height, and λ (linear) wavelength.

2. Theoretical model of the membrane solar island

We define an Earth-fixed coordinate system with the origin in the center of the model. $z = 0$ coincides with the still water surface and the positive direction of z is upwards. See Figure 4. The floater is assumed

to be half-submerged and with radius R, so that $r = R, z = 0$ corresponds to the center-axis of the floater. The cross-sectional diameter of the floater is $2a$. The membrane is modelled as a disk with 0.001 m draft and radius $R_0 = 0.46$ m, corresponding to the membrane thickness, and the horizontal part of the membrane lying on the water. There is thus in the physical model a small gap of width $R - R_0 - a = 0.034$m between the membrane and the floater.

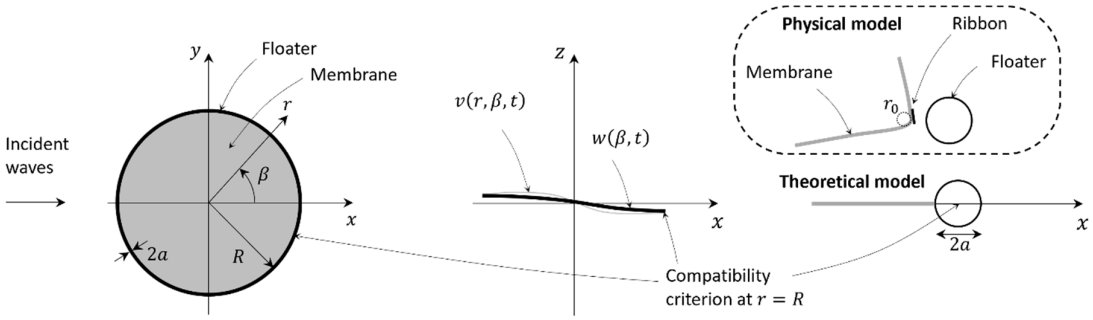

Figure 4. Schematic illustration of the theoretical model of the solar island. Both the membrane and floater are assumed to undergo small vertical motions, v and w relative to the model diameter $2R$. In our theoretical model, a compatibility criterion is imposed at the center-axis of the floater, $r = R$. In the physical model, the membrane is fixed to the torus by steel clips and a ribbon, there $0.034m$ gap between the floater and membrane, and there is a curved part of the membrane with radius $r_0 \simeq 0.01m$.

We focus on the vertical, flexible motions of the island. Surge of both the membrane and floater is also included in the analysis, due to coupling with pitch motion. A two-body approach is taken: the membrane and the floater. The two bodies interact both structurally and hydrodynamically. The vertical motions of both the floater and membrane are assumed small relative to the model diameter. The vertical floater motion is represented by a modal decomposition, as

$$w(\beta, t) = \sum_{m=0}^{\infty} a_m(t) \cos m\beta. \tag{1}$$

Here, $a_m(t)$ are time-dependent modal weights, and we have included terms proportional to $\cos m\beta$ only (and not $\sin m\beta$) with the assumption that waves travel along the x-axis without loss of generality. The vertical membrane motions are decomposed into corresponding Fourier-Bessel modes, as

$$v(r, \beta, t) = \sum_{m=0}^{\infty} \sum_{n=1}^{\infty} b_{mn}(t)\, J_m(\mu_{mn} r) c_{mn} \cos m\beta. \tag{2}$$

Here, J_m is the Bessel function of the first kind and μ_{mn} satisfy zero Neumann conditions at the membrane rim, $\partial J_m(\mu_{mn}R)/\partial r = 0$. The index n denote subsequent roots with $n = 1$ corresponding to the first. $c_{mn} = J_m(\mu_{mn}R)^{-1}$ is a normalization factor chosen such that all modal values attain unit value at the membrane rim. Note that, because of this choice of normalization, the maximum value of the modes is in general higher than unity. For instance, a value of $b_{02} = 0.4$, means that the vertical motion of this mode is approximately 1 at the model center. Using Dirichlet condition modes, so called drumskin modes, would not allow for any membrane motion at the rim. A combination should have been used, however, since the Neumann modes allows for no vertical loads to be absorbed radially, since a membrane can only absorb internal loads tangentially. This can be considered as further development. The torus vertical motions are assumed to obey the modified Euler beam model [5],

$$m_f \frac{\partial^2 w}{\partial t^2} + EI \frac{\partial^4 w}{\partial s^4} + \frac{EI}{R^2} \frac{\partial^2 w}{\partial s^2} - \frac{\partial}{\partial s}\left(T_{ax} \frac{\partial w}{\partial s}\right) = f - 2\rho g a w. \tag{3}$$

Here $m_f = 0.5\rho\pi a^2$ is the structural mass per unit length of the floater, EI the total bending stiffness, and f represent the external forces; wave excitation loads, added mass and damping loads and point loads by moorings. The total bending stiffness accounts for both the floater and ribbon bending stiffnesses, i.e. $EI = EI_f + EI_m R^4/R_0^4$. $T_{ax}(s)$ is the axial tension in the torus. In the present work, this is assumed zero. The hydrostatic restoring load is given explicitly as $-2\rho g a w$. This is given that the floater is half-

submerged in static conditions. However, in the tests the floater draft was slightly less, approximately $0.8a$, and this must be considered an uncertainty in our model. The membrane is modelled by the pre-tensioned, linear membrane equation

$$m\frac{\partial^2 v}{\partial t^2} - T_0\left(\frac{\partial^2 v}{\partial r^2} + \frac{1}{r}\frac{\partial v}{\partial r} + \frac{1}{r^2}\frac{\partial^2 v}{\partial \theta^2}\right) = q(r,\theta,t), \qquad r \le R \tag{4}$$

where m is the structural mass per unit area of the membrane, T_0 is the pre-tension per unit length of the membrane and q is the external vertical force per unit area of the membrane. This is a linear equation that is violated if the membrane goes slack. In the present model tests the membrane was sufficiently pre-tensioned such that slack was not observed during tests. The mooring is modelled as linear, pre-tensioned springs in the surge and pitch equations of the floater.

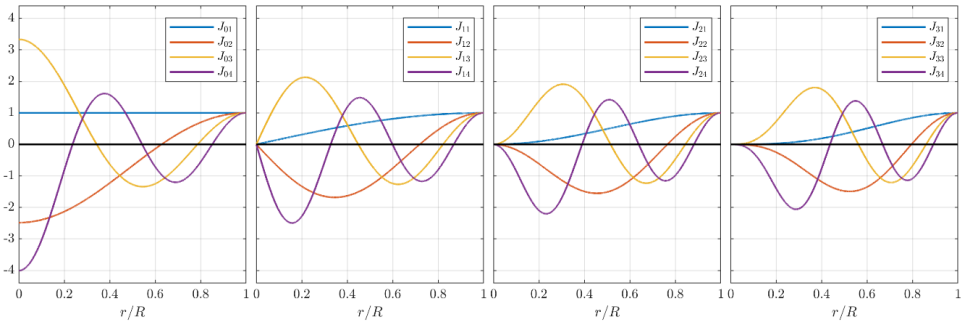

Figure 5. Radial variation of selected membrane modes $J_{mn}(\mu_{mn}r)c_{mn}$. Note that only the lowest azimuthal modes, $m = 0$ attain a non-zero value at the origin, and that $m = 0, n = 1$ represents heave of the membrane.

We solve the problem in frequency domain, assuming linear potential flow theory to be valid and that all quantities behave sinusoidally with wave frequency ω. The incident wave direction is along the positive x −axis. We use the method of generalized modes in WAMIT 7.4. This means we compute generalized wave excitation loads, added mass and damping coefficients and hydrostatic restoring coefficients by WAMIT. We truncate the modal representations (1) and (2) to M azimuthal and N radial modes. The number of unknowns includes surge of both the membrane and the floater, M vertical torus modes and $M \times N$ vertical membrane modes, $N_t = M(N+1)+2$. Next, (1) is inserted into (3), multiplied by torus modes $p = 0,..,M-1$ and integrated along the torus. Similarly, (2) is inserted into (4), integrated by membrane modes with couples $pq = (0,..,M-1)(1,..,N)$ and integrated over the membrane. All the dry membrane modes, (2), are orthogonal. However, for a given m, all N membrane modes are hydrodynamically coupled. The resulting linear system of equations can be expressed in the commonly used way as

$$\boldsymbol{K\eta} \equiv [-\omega^2(\boldsymbol{M}+\boldsymbol{A}) + i\omega\boldsymbol{B} + (\boldsymbol{C}+\boldsymbol{C}_m)]\boldsymbol{\eta} = \boldsymbol{F}, \tag{5}$$

where $\boldsymbol{M}$ is the generalized (dry) mass matrix, $\boldsymbol{A}$ and $\boldsymbol{B}$ are the generalized added mass and damping matrices, $\boldsymbol{C}$ the generalized hydrostatic restoring matrix, $\boldsymbol{C}_m$ the generalized structural stiffness matrix involving the floater bending stiffness EI_f, the membrane ribbon bending stiffness EI_m, and the membrane pre-tension T_0, and $\boldsymbol{F}$ the generalized wave excitation loads. The vector $\boldsymbol{\eta}$ represents the unknown surge and vertical modal weights. So far, the two bodies are not structurally connected. The structural coupling of the membrane and floater is modelled in a simplified manner. Rather than modelling all the details related to steel clips and rubber bands, we impose the coupling constraint that the vertical and horizontal motion of the membrane rim is equal to the vertical floater motion at its center axis, $w(\beta,t) = v(R,\beta,t)$, so that from (1) and (2) we get

$$\sum_{n=1}^{N} b_{mn}(t) = a_m(t), \qquad m = 1,2,\dots,M. \tag{6}$$

This may be expressed in a compact form as $\boldsymbol{D\eta} = 0$. The membrane and floater must thus obey their respective equations of motion (3) and (4) and the coupling constraint (6). We employ the standard method

of using Lagrangian multipliers to achieve this, as exemplified by [6]. It involves satisfying taking the first variation of the Lagrangian functional,

$$L = 0.5\boldsymbol{\eta}^T\boldsymbol{K}\boldsymbol{\eta} - \boldsymbol{\eta}^T\boldsymbol{F} + \boldsymbol{\lambda}^T\boldsymbol{D}\boldsymbol{\eta}. \quad (7)$$

That is, the partial derivatives of L with respect to all η_i and λ_i must be zero. Since $\boldsymbol{D\eta} = 0$, this recovers the equation of motion if $\boldsymbol{K}$ is symmetric. It also provides the solution for all Lagrangian multipliers, which represent the generalized modal contact loads between the membrane and the floater. The method provides a practical and rational way to enforce equal motion of the floater and membrane at the membrane rim but cannot be expected to be a good representation if detailed analysis of the outer membrane part is needed. Due to hydrodynamic coupling between n-modes and the coupling constraint (6), a system of equations involving all the unknowns simultaneously must be solved. The total number of unknowns in our final linear system of equations, (7) , is therefore the number of body modes N_t plus the N Lagrangian multipliers. We emphasize that the presented model is linear in all aspects. Nonlinear effects are, however, expected to matter, such as both structural and hydrodynamic nonlinear damping, over-topping of waves on the floater, floater and membrane partly going out of water and nonlinearities related to the wrapping of the membrane.

3. Results and discussion

We discuss results in terms of modal and pointwise RAOs, i.e. the ratio between the response amplitude and incident wave amplitude. The (basic harmonic) incident wave amplitude ζ_a is estimated as the mean amplitude of band-pass filtered time-series from wave gauges 1 and 2 (Figure 1) in near steady-state time-windows in tests with model. The time-series are band-pass filtered around the basic frequency, ω, of the incident wave. For $kR > 2$, time-windows prior to reflections from the model are possible. For $kR > 3.5$, time-windows of responses prior to beach reflections are possible. Typical beach reflections are in the range $5 - 10\%$ of the incident first harmonic wave amplitude, based on prior investigations.

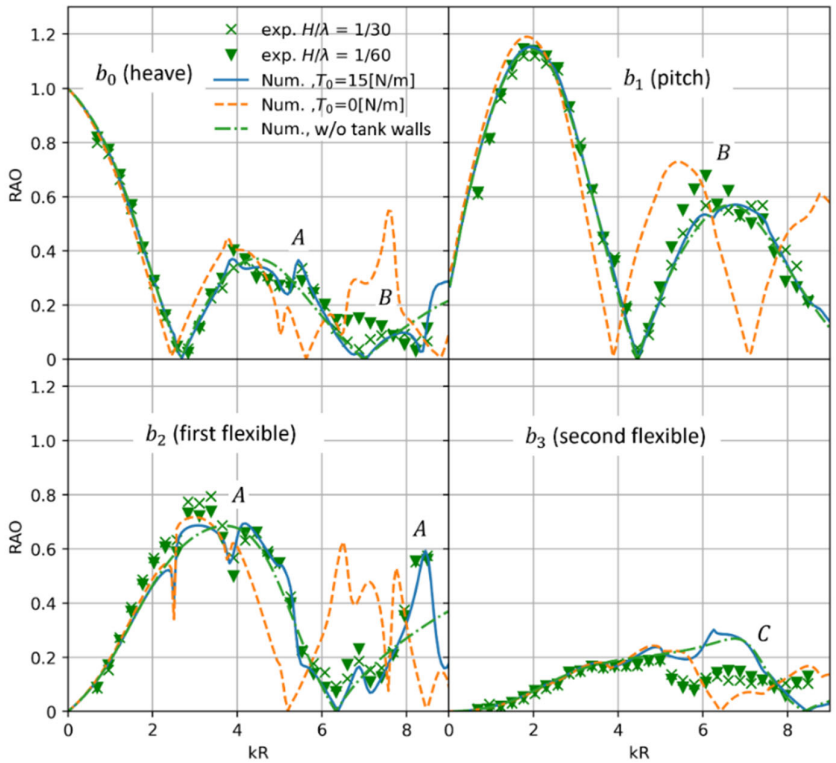

Figure 6. Modal RAOs for the four lowest floater modes, $m = 0, 1, 2$ and 3. The experimental values are provided as mean values and standard deviation. The standard deviate includes both wave steepnesses $H/\lambda = 1/30$ and $1/60$ and repetition tests. Numerical results are provided both with zero membrane pretension, and with the pretension given as our best estimate, $T_0 = 15$ N/m.

Our numerical results are all computed with $M = N = 5$, i.e. 25 membrane modes and 5 torus modes. This is done from practical reasoning, by first investigating the error in modal reconstruction of the membrane and floater vertical motions from the regular wave tests. For $kR < 4$, the maximum error over the whole measured area of the membrane is less than 3%. For $kR > 4$, the error is less than 6%. Including up to $M = N = 9$ modes does not improve this significantly, but $M = N \leq 4$ results in a rapid increase in the error with decreasing number of modes. Similar observations are made for the floater. The membrane has draft 0.001m and radius $R_0 = 0.46$m. We have not investigated possible gap resonances, but there is no sign of this in the responses we have studied in the investigated wave frequency range. Structural damping is neglected, although it may have importance.
The first four floater mode RAOs are presented in Figure 6, as function of non-dimensional wave number kR. Here, k is the wave number obeying the linear dispersion relation accounting for finite water depth h. From the figure we make four main observations. First, membrane pre-tension matters significantly. Zero membrane pre-tension must be seen theoretically as the limit with infinitesimally small motions and with a corresponding infinitesimally low pre-tension to avoid slack. A low pre-tension will allow slack and possibly resulting, unwanted snap loads. It was difficult to measure the membrane pre-tension in the experimental set-up. Attempts were made by measuring the lowest drumskin mode natural frequency. Our best estimate was $T_0 = 12 - 18$ N/m. $T_0 = 15$ N/m gives the best comparison to the experimental values, and this value is used throughout the rest of the study.

Next, the wave steepness matters non-negligibly, for which we have not been able to provide any definite reason. Repetition tests performed two months after the DIC measurements show significantly less wave steepness effects. Tank wall reflections give rise to irregularities in the response curves (marked A in the figure). Third, the amount of nonlinearity is modest, although not negligible (B). Last, the numerical predictions are in general in fair agreement with the experiments, except for the second flexible mode for short waves (C).

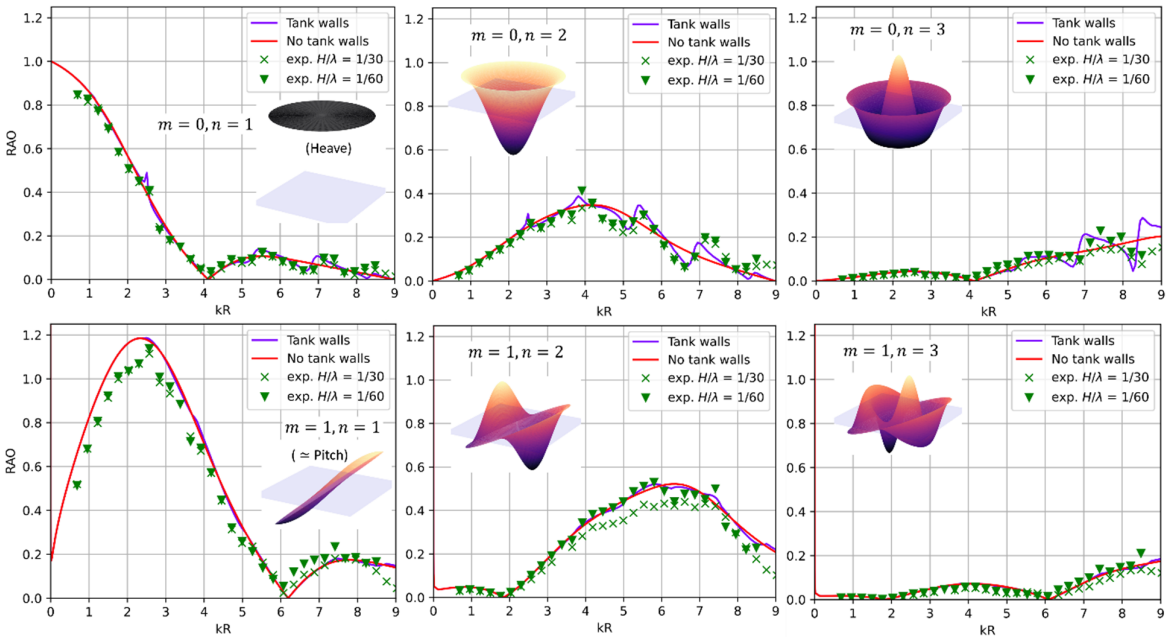

Figure 7. Selected membrane mode RAOs for the three lowest symmetric $(m = 0)$ modes and three lowest antisymmetric $(m = 1)$ modes. For these modes, there is fair agreement between the numerical predictions and experimental data. Some non-negligible nonlinearity is observed for $m = 1, n = 2$.

Selected membrane mode RAOs for low modes are presented in Figure 7. Similar comments apply as for the floater modes: the numerical predictions are similarly affected by membrane pre-tension (not shown) as for the torus modes, tank wall effects are present, there are some effects of wave steepness, but rather limited, and the agreement is in general quite fair.

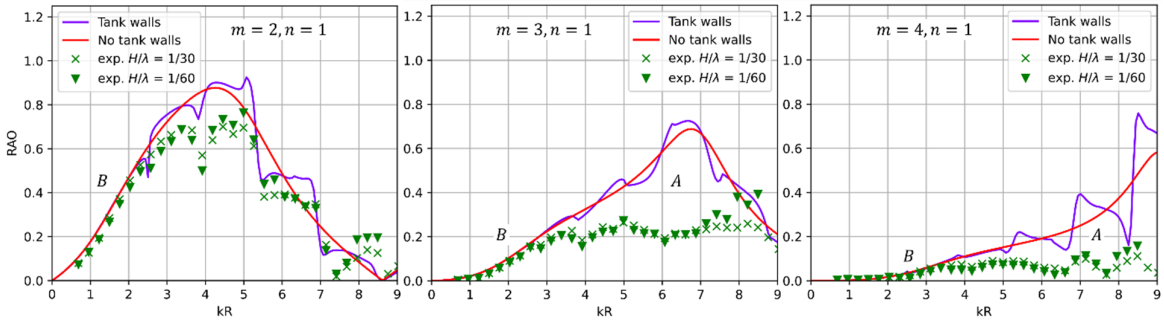

Figure 8. Selected membrane RAOs for modes with higher azimuthal variation, $m = 2, 3$ and 4. For these membrane modes, significant discrepancies occur for some wave numbers. There are clear nonlinearities indicated for some wave numbers.

In Figure 8 we illustrate, however, that the agreement is not good for waves that are shorter than the model diameter, $kR \geq 3$ for higher membrane modes. This is most applicable to modes $m = 3$ and $m = 4$, with $n = 1$ (A). We attribute these discrepancies to an insufficient representation of the outer part of the membrane in relation to the way the floater and membrane are connected in our theoretical model relative to that in the physical model. For waves with wavelength in the order of the diameter of the model or longer, $kR \leq 3$, the agreement is in general quite good also for these modes (B). All other modes (not presented) are quite low valued, with RAOs less than about 0.1 for long waves, $kR \leq 3$. This means that our theoretical model is fair for long waves, $kR \leq 3$. For responses such as wave-overtopping, the structures' ability to follow the waves is the essence, and long waves are most important in this respect due to their potentially large wave heights. For local responses of the membrane related to for instance snap loads and connections, short waves will be important.

We illustrate how the insufficient theoretical modelling of the membrane-floater connection affects the predicted motions of the membrane for short waves by studying the vertical motion RAOs along the centerline of the model, $y = 0$. See Figure 9 for three selected wave numbers. The motions are reasonably predicted for $kR = 3.11$, where the wavelength is roughly the same as the model diameter. There are notable discrepancies for $kR = 5.0$; the overall behavior is reasonable with a main exception at the rear side (A), which is close to the rim of the membrane. For the largest wave number, $kR = 6.87$, for which there are more than two wave lengths across the model diameter, the discrepancies are significant (B); the numerical curves seem shifted relative to the experimental curves.

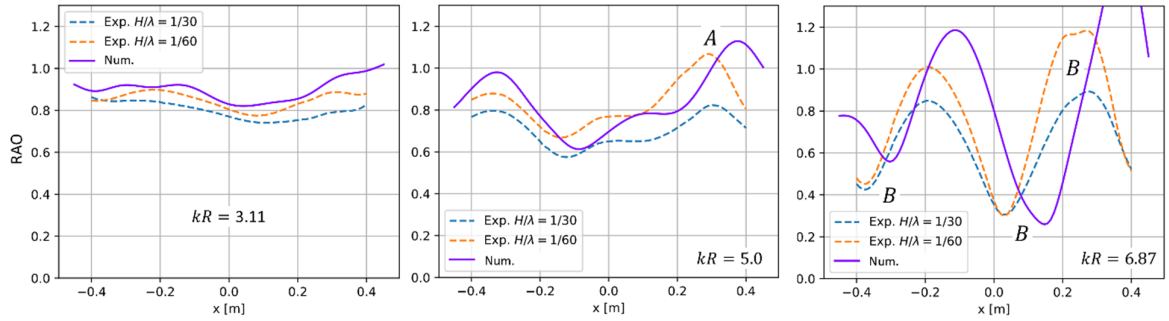

Figure 9. Membrane vertical motion RAOs along the centerline $y = 0$. The experimental values are taken directly from the DIC measurements (199 data points for the range $x = \pm 0.4$ m).

We illustrate further how pointwise motions are predicted, by studying motions at selected points on the membrane and the floater as function of wave number. See Figure 10. We first consider the point at the membrane center, $x = 0, y = 0$. The numerically predicted motions are in rather fair agreement with the experiments, considering the relatively complex, elastic model and tank wall effects. The wave steepness matters non-negligibly, and as mentioned earlier, we have not been able to identify main reasons for this.

Next, focusing on the membrane front part, $x = -0.4, y = 0$, the predictions are fair for $kR \leq 6$, (A), whereas large discrepancies occur for larger wave numbers (B). This point is close to the membrane rim, and recall that the membrane wrapping occurs at $x = -0.45$ m. For the aft of the membrane, $x = 0.4$ m, $y = 0$ m, the situation is even worse. The numerical predictions are far from the experimental values for $kR \geq 4$, (C). It may seem from this that there are errors or non-converged numerical results. However, we explain this by the results presented in Figure 9; the large discrepancies are related to rapid spatial variations, and therefore high spatial sensitivity. The high spatial sensitivity combined with an insufficient theoretical representation of the membrane/floater connection explain to our understanding the large discrepancies in this point RAO. Another observation is that the RAO does not tend to unity as $kR \to 0$ at the rear (D), as one should expect, and as is the case in the front of the model (left subfigure). Although beach reflections may be part of the reason, we have not found a complete explanation for this. Calibration of the DIC cameras may be one cause.

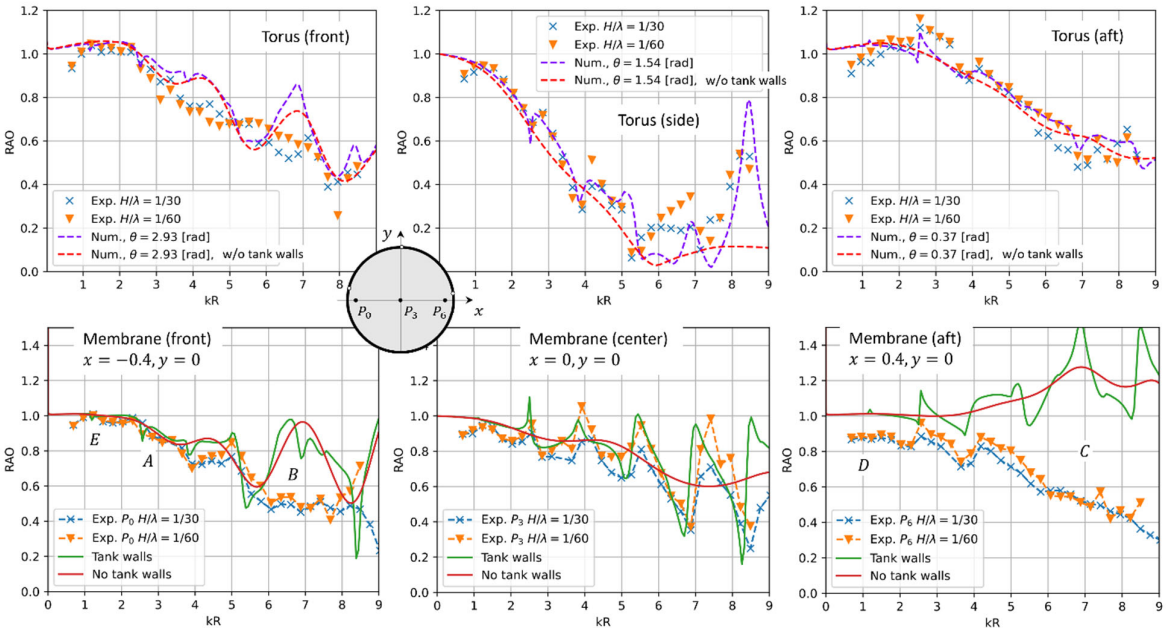

Figure 10. Pointwise vertical membrane motion RAOs for selected points on the membrane and floater. Incident waves are along the positive x-axis. The experimental values are taken directly from Oqus (floater) and DIC (membrane), i.e. not from modal reconstruction. The numerical and experiments are in fair agreement at the membrane center, but there are clear and large discrepancies at the front and aft of the membrane for $kR \geq 5$. We attribute this mainly to that representation of the outer part of the membrane is insufficient in our theoretical model.

We performed sensitivity studies with respect to several parameters, including membrane pre-tension T_0, bending moment of the torus/ribbon, torus cross-sectional diameter, membrane radius, number of modes $M = N$, including or excluding the effect of mooring in the surge and pitch equations of motion, and combinations of these. None of the variations provided improved results in general. Therefore, we believe that the representation of the membrane connection to the floater is essential to progress towards a more accurate model for short waves. One suggestion to improve the membrane/floater connection rationally is to include an additional curved Euler-Bernoulli beam representing the bending stiffness by the ribbon/membrane wrap at the actual position of the ribbon, $R_0 = 0.46$ m and model the connections to the flexible floater by rigid rods allow to move in local heave and pitch. In addition, modelling of nonlinear effects such as those mentioned earlier in the paper is needed.

We last present snapshots from numerical predictions of the membrane and floater for three selected wave numbers. See Figure 11. The snapshots illustrate two main facts. One is that the coupling constraint between the membrane and floater are correctly implemented, i.e. that the membrane rim at $r = R$ is equal to the torus center-axis motion. The other is that the membrane motions are exaggerated near the membrane rim for the two highest wave numbers, as discussed above. For $kR = 7.13$, it appears visually that for instance the membrane mode $m = 3, n = 1$ represents a major part of the exaggerated motion, consistent with the modal RAOs presented in Figure 8.

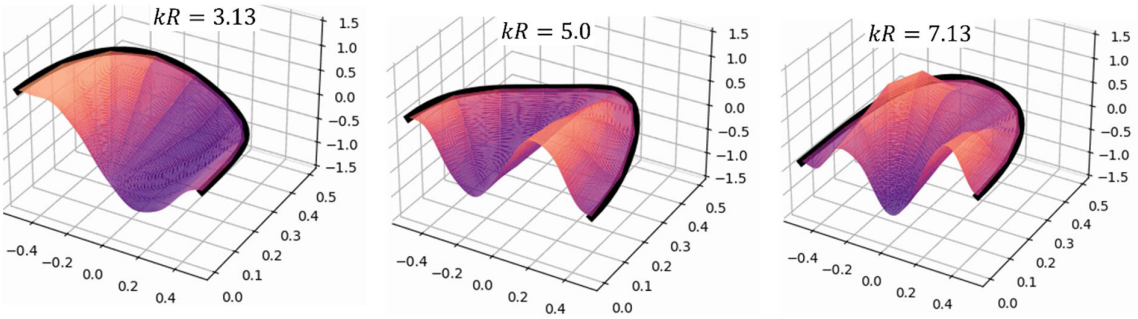

Figure 11. Snapshots from simulations of the membrane and the floater for three selected values of non-dimensional wave number kR.

4. Conclusions

We have presented work towards a rational model of a circular, floating membrane solar island. Our model is linear in all aspects, based on a modal approach and solved in the frequency domain. The hydrodynamic problem is solved by generalized modes using WAMIT. The elastic floater is modelled as a curved Euler-Bernoulli beam. The membrane is modelled by the pretensioned membrane equation. The coupling between the membrane and the floater is modelled in a simplified manner by Lagrangian multipliers. Our focus was on the (flexible) vertical motions. Dedicated model tests were performed using optical measurement devices. Our model was able to predict quite well the vertical motions of both the floater and the membrane for waves in the order of the model diameter or longer. A better modelling of the connections and improved modal representation is needed for short waves.

Acknowledgements

This work was partly supported by the Research Council of Norway through SFI BLUES, grant number 309281 as well as NTNU AMOS, grant number 223254. We acknowledge OceanSun (Patent numbers WO2017/209625, WO2020/040643) for partly supporting one of the co-authors.

References

[1] O. J. Waals, T. H. J. Bunnik and W. J. Otto, *Model Tests and Numerical Analysis for a Floating Mega Island*, OMAE, Madrid (2018)
[2] T. Kristiansen, M. V. Sigstad, J. Winsvold, Ø. Rabliås and O. M. Faltinsen, *A flexible multi-torus solar island concept*, IWWWFB, digital workshop (2021)
[3] B. Bjørneklett, *Offshore floating solar – a technical perspective,* PV Tech Power Volume, 16, pp. 60-64, (Sep. 2018)
[4] R. Mondal, S. Mandal ant T. Sahoo, *Surface gravity wave interaction with circular flexible structures*, Ocean Engng., 88 (2014
[5] Peng Li, O. M. Faltinsen and M. Greco. *Wave-Induced Accelerations of a Fish-Farm Elastic Floater: Experimental and Numerical Studies*. J. Offshore Mech. Arctic Engng. 140, 1 (2017)
[6] L. Sun, R. Eatock Taylor and Y. S. Choo, Responses of interconnected floating bodies, IES J. Part A: Civil and Struct. Engng., 4, 3, (2011)